

Why is gallium-doped silicon (sometimes) stable? Kinetics of light and elevated temperature induced degradation

Fabian T. Thome^{a,*}, Cem Yilmaz^a, Wolfram Kwapil^{a,b}, Florian Schindler^a, Martin C. Schubert^a

^a Fraunhofer Institute for Solar Energy Systems (ISE), Heidenhofstr. 2, Freiburg im Breisgau, 79110, Germany

^b Department of Sustainable Systems Engineering (INATECH), Emmy-Noether-Straße 2, Freiburg im Breisgau, 79110, Germany

ARTICLE INFO

Keywords:

Gallium-doped
Light and elevated temperature induced degradation (LeTID)
Czochralski silicon
Photovoltaics
p-type
Accelerated testing

ABSTRACT

Light and elevated temperature induced degradation (LeTID) can induce high power losses in photovoltaic modules built from various types of silicon wafers. After the industry's rapid transition from Boron- to Gallium-doping, it is still unclear how the new dopant atom affects the degradation process and why it entails an apparently higher resistance to LeTID. We treat identically processed Gallium-doped Czochralski silicon wafers at 16 different conditions by screening temperature and minority charge carrier density (in the following "injection"). The illumination source is regulated to keep the injection constant at each condition. This method allows for an improved quantitative analysis of the LeTID kinetics based on effective lifetime measurements. Our results show that Gallium-doping shifts the equilibrium between the formation of LeTID defects and their temporary recovery (TR) to the latter, leading to a reduced degradation extent at temperatures up to 80 °C. The efficacy of this TR-induced LeTID suppression depends delicately on both temperature and injection which explains why Gallium-doped silicon appears to be LeTID-immune at high illumination intensities. By accounting for the influence of TR, we extract activation energies and injection exponents that relate to the dominant defect transitions separately, revealing a large discrepancy to effective values reported in literature. The increased accuracy of our kinetic parameters enhances the reliability of existing efficiency models. Finally, we find that a degradation as expected under field conditions can be probed at a 100-fold accelerated rate in the lab. By shining light on LeTID kinetics in Gallium-doped silicon, we explain the dopant atoms' influence on the degradation behavior, establish a basis for precise yield modelling and formulate guidelines for accelerated test protocols.

1. Introduction

P-type Czochralski-silicon (Cz-Si) is currently the photovoltaic industry's working horse and will likely continue carrying a major part of the worldwide production for the next five to ten years on its shoulders [1]. To secure crucial investments for the rapid expansion of deployment capacity, stability-compromising degradation processes must either be avoided completely or understood well enough that a precise risk assessment is possible. Degradation via the formation of Boron-Oxygen-defects has already been circumvented by substituting Boron with Gallium as the dopant atom [1–3]. A second degradation process however, known as light and elevated temperature induced degradation (LeTID) [4], is present for both these dopants [5,6].

LeTID is a bulk effect common in multicrystalline (mc)- [4,7–10], Cz- [11,12] and floatzone- [13–15] silicon with a potential module power loss of 7 %_{rel} under test conditions relating to just a few years of field

installation in mc-Si [16]. The degradation extent was found to depend on the efficacy of hydrogen diffusion from the surface passivation layers into the silicon bulk during contact firing [17–22]. Controlling the bulk hydrogen concentration by adapting the firing conditions [23–26], the wafer thickness [22,27,28] or the passivation layer stack [29–33] has proven to be a promising route towards the suppression of LeTID for both Boron- and Gallium-doped silicon (Si:B, Si:Ga) wafers and solar cells [34,35]. However, hydrogenation is essential for an excellent defect passivation required in high efficiency solar cells [36], indicating these mitigation strategies could pose a limitation in yield optimization.

Despite the processes' otherwise ubiquitous nature, the choice of dopant atom critically affects the LeTID kinetics. Most prominently, LeTID occurs in Si:Ga at a much slower pace and seemingly with an intrinsically lower degradation extent than in Si:B [5,6,37,38]. Furthermore, LeTID was found in Si:B when subjected to a wide range of injections [10], whereas Kwapil et al. reported a lack of degradation at

* Corresponding author. Heidenhofstr. 2, 79110 Freiburg im Breisgau, Germany.

E-mail address: fabian.thome@ise.fraunhofer.de (F.T. Thome).

increased injection for Si:Ga [5]. The authors suspected that the reverse transition to degradation, i.e. temporary recovery (TR), could effectively suppress degradation in Si:Ga even at elevated temperatures ($\sim 75^\circ\text{C}$) as long as the injection is sufficiently high. However, an extensive investigation of the injection and temperature dependence of LeTID kinetics, as was done for Si:B [10,26,39–41], is still missing for Si:Ga. This is also reflected in the wide range of activation energies (0.58–0.90 eV) found in the literature specific to Si:Ga [19,26,41–43].

Investigating LeTID kinetics in Si:Ga is a prerequisite for deployment-location specific yield modelling, the formulation of well-defined test protocols with which LeTID could reliably be recognized and assessed, and finally, a deeper understanding of LeTID at the atomic level. We therefore systematically study the injection- and temperature dependence of LeTID in Si:Ga. Our findings explain why Si:Ga degrades less than Si:B at specific treatment conditions and how this can lead to the perception of a dopant-induced LeTID immunity. We also provide improved kinetic parameters for modelling LeTID in Si:Ga and reveal the origin of the wide span of activation energies reported in the literature. Finally, guidelines for accelerated testing are established that should serve as a basis for industrial test-protocols.

2. Theory

The formation of recombination-active defects can be tracked using the normalized defect density $\text{NDD}(t, \Delta n) = \frac{1}{\tau_{\text{eff}}(t, \Delta n)} - \frac{1}{\tau_{\text{eff}}(t_0=0, \Delta n)}$, which is defined via the effective lifetime of minority charge carriers τ_{eff} [44]. We assume direct proportionality between NDD and the LeTID defect density, implying that the recombination by other mechanisms is unchanged throughout the experiments. Downfalls to this approach could be the splitting of iron-gallium-pairs or the onset of surface recombination. Precautions to minimize the impact of both aspects will be detailed in section 3.

The LeTID cycle is well described by the three-state-model initially devised for boron-oxygen-degradation [45,46]. The actual degradation is the transformation of recombination-inactive LeTID precursors (state A) to recombination-active LeTID defects (state B) during light and temperature intensive treatment. The degradation is for Si:B characterized by an Arrhenius-like temperature activation coupled with an approximately linear injection dependence [10]. TR is the reverse process to degradation and appears in both Si:Ga and Si:B [5,39]. A study on mc-Si:B solar cells suggests a much weaker temperature activation but a stronger, i.e. approximately quadratic, injection dependence for TR [39]. The LeTID defects can also regenerate into state C which is stable against the typical degradation conditions.

The populations of the precursors, defects and regenerated species are within the framework of the three-state-model described with a system of differential equations,

$$\frac{dA(t)}{dt} = -k_{AB}A(t) + k_{BA}B(t), \quad (1)$$

$$\frac{dB(t)}{dt} = k_{AB}A(t) - k_{BA}B(t) - k_{BC}B(t), \quad (2)$$

$$\frac{dC(t)}{dt} = k_{BC}B(t), \quad (3)$$

where the transition rate coefficients k_{ij} determine the temperature and injection dependence:

$$k_{ij}(T, \Delta n) = \nu_0 \left(\frac{\Delta n}{\Delta n_0} \right)^{x_{ij}} \exp\left(-\frac{E_a^{ij}}{k_B T}\right). \quad (4)$$

Here, the subscripts i and j represent the different states A, B or C, ν_0 denotes an attempt frequency, the injection exponent x_{ij} can be understood as the stoichiometric factor in a minority charge carrier-driven reaction, $\Delta n_0 = 1\text{cm}^{-3}$ is introduced for normalization and the activa-

tion energy E_a^{ij} as well as the Boltzmann constant k_B appear in the characteristic Arrhenius-law. While an Arrhenius-like temperature dependence has been found for both degradation and regeneration, it appears not to be descriptive of TR, for which Kwopil et al. reported a decrease of the rate coefficient with increasing temperature [39].

The differential equations (1)–(3) can be solved for an analytical expression of $B(t)$ [46], although extracting transition rate coefficients from a fit to an NDD(t) curve is only possible if the number of free fit parameters is reduced by taking approximations. Frequently, e.g. Refs. [26,41,47,48], the rise-to-maximum function

$$\text{NDD}(t) \propto B(t) \stackrel{\text{def}}{=} \text{NDD}_{\text{max}}(1 - \exp(-k_{\text{eff}}t)) \quad (5)$$

is used for fitting and the effective transition coefficient k_{eff} is interpreted as the pure degradation rate coefficient k_{AB} . This method of analysis is only valid if neither TR nor regeneration are significant, i.e. $k_{BA} \approx 0$ and $k_{BC} \approx 0$. As will be shown in section 4, this is almost never the case for Si:Ga and hence care should be taken with such interpretations. We instead focus on cases where degradation is accompanied by just one other transition, i.e. $k_{BC} \approx 0$ or $k_{BA} \approx 0$.

In the case of negligible regeneration ($k_{BC} \approx 0$) but significant TR, solving the differential equations yields

$$B(t) = \frac{k_{AB}A_0}{k_{AB} + k_{BA}}(1 - \exp(-(k_{AB} + k_{BA})t)), \quad (6)$$

with the initial LeTID precursor population $A_0 = A(t=0)$. Since equations (5) and (6) can take the same shape, NDD curves alone are insufficient to differentiate between pure degradation and mixtures of degradation and TR. This requires additional information for example in the form of the precursor density A_0 . The parameter A_0 is expected to correlate with the bulk density of molecular hydrogen [19,21,22] but its value in NDD-units (s^{-1}) cannot be measured directly. It will be explained in section 4.3 how we obtain A_0 to utilize equation (6) instead of equation (5) nonetheless.

In the case of negligible TR ($k_{BA} \approx 0$) but significant regeneration, the three-state-model yields a description of $B(t)$ via two independent exponential functions:

$$B(t) = \frac{k_{AB}A_0}{k_{AB} - k_{BC}}(\exp(-k_{BC}t) - \exp(-k_{AB}t)). \quad (7)$$

If $k_{AB} \gg k_{BC}$, the rising edge of equation (7) can resemble rise-to-maximum behavior as well. An associated fit to equation (5) requires less data and thus less experimental effort but is only justified if k_{AB} is at least two orders of magnitude larger than k_{BC} (see Supplementary Fig. 1). The influence of regeneration at times of effective lifetime degradation otherwise prevents correct fitting. Importantly, the degradation and regeneration rate coefficients are, according to our dataset, never apart by a factor higher than 10. Fits of equation (5) to a rising edge of the LeTID cycle are thus in general not sufficient to extract information on k_{AB} . Instead, the full LeTID cycle should be probed and equation (7) should be used for fitting.

3. Experimental details

3.1. Sample processing

In this study, we focus mainly on one group of samples that were all processed identically. Cz-Si:Ga M2 wafers with a base resistivity of 0.69 Ωcm from Longi were first saw-damage-etched and cleaned before undergoing a gettering-step via POCl_3 diffusion and the subsequent back-etching of both the phosphosilicate glass and the emitter. A 100 nm passivation layer of hydrogen-rich silicon nitride (SiN_x) with a refractive index of $n = 2.05$ was afterwards deposited symmetrically on both sides using a c.PLASMA 2.600 from Centrotherm. The wafers were then fired at a measured peak temperature of 800°C and our standard cooling

ramp of ca. 80 K/s [34]. This processing sequence ensures a high hydrogen concentration in the bulk that is comparable for all investigated samples. The wafers were afterwards cleaved into quarters of equal size for the LeTID tests. Si:B floatzone M2 wafers with a base resistivity of 2.8 Ωcm underwent identical processing and serve as a reference group. The median effective lifetime after firing evaluated at 60 °C and $\Delta n = 2 \times 10^{14} \text{cm}^{-3}$ was 250 μs and 420 μs with standard deviations of 20 μs and 40 μs for the Cz-Si:Ga and Si:B floatzone samples, respectively.

3.2. Degradation at constant minority charge carrier density

Without any further thermal preconditioning that could alter the LeTID kinetics [49], the samples were placed on precision hot plates (Präzitherm) under light emitting diode (LED) lamps. Injection dependent effective lifetime curves were measured ex-situ with a Sinton Instruments lifetime tester WCT-120TS at the respective treatment temperature. This allows to calculate the minority charge carrier density of a sample during a LeTID test from a given generation (via $G = \frac{\Delta n}{\tau(\Delta n, T)}$). The illumination of the LEDs was regulated after each lifetime measurement to reach a generation that corresponds to an injection close to a targeted value throughout the complete treatment. A similar approach was previously applied by Graf et al. for Si:B [48] and most recently also by Zerfuß et al. for Si:Ga [19]. We demonstrate with a proof-of-concept experiment (see Supplementary Fig. 2) that this approach is crucial for a precise determination of kinetic parameters and should thus be adopted by all studies aiming at a quantitative understanding of LeTID kinetics.

Despite the gettering step, some wafers featured a detectable iron contamination determined as $(2.2 \pm 0.6) \times 10^9 \text{cm}^{-3}$ using the defect parameters given in Ref. [50]. Thus, the samples were flashed with the lifetime tester until the effective lifetime value was stable before taking the actual measurement. Also, care was taken to measure the samples right after removing them from the hot plate (i.e. within 10 s). The effective lifetime was always evaluated at $\Delta n = 2 \times 10^{14} \text{cm}^{-3}$, a value

close to the observed cross over point at 60 °C. This further reduced the impact of iron contamination on our evaluation.

Following the description of Hammann et al. [51], the recombination parameter j_{0s} was extracted from lifetime data. Aside from minor fluctuations, the value remained constant throughout the whole treatment. Hence, the NDD can be seen as a good proxy for the LeTID defect density.

4. Results

4.1. Temperature and injection screening

To study the temperature and injection dependence of LeTID transitions, the Cz-Si:Ga samples were treated at four temperatures (60, 80, 100 and 120 °C) and four injections ($0.7, 1.34, 2.59$ and $5 \times 10^{15} \text{cm}^{-3}$), giving a total of 16 treatment conditions.

The four panels of Fig. 1 show the measured NDD for each injection with the temperature color coded. Lifetime degradation is apparent in all cases except for the combination of lowest temperature and highest injection. Here, the NDD remains close to zero for over 50 h, indicating that only few defects have formed. The degradation speed increases strongly with temperature, confirming that degradation is a thermally activated process. The maximum degradation extent increases as well, but it appears to be limited for 100 °C and 120 °C at an NDD of about 30ms^{-1} by the onset of regeneration. At lower temperatures, i.e. 60 °C and 80 °C, the NDD begins to saturate already at lower values (except for 80 °C, $0.7 \times 10^{15} \text{cm}^{-3}$) that depend strongly on both temperature and injection.

To highlight the injection dependence of the LeTID kinetics, the NDD-data is replotted in Fig. 2 with a panel for each temperature and the injection color coded. This representation underlines that at 100 °C and 120 °C, the LeTID cycle proceeds much faster for higher injections while the degradation maximum shows no obvious injection dependence. At 60° and 80 °C, a higher injection causes a faster initial increase of NDD, while the maximum degradation extent is reduced. This forces the

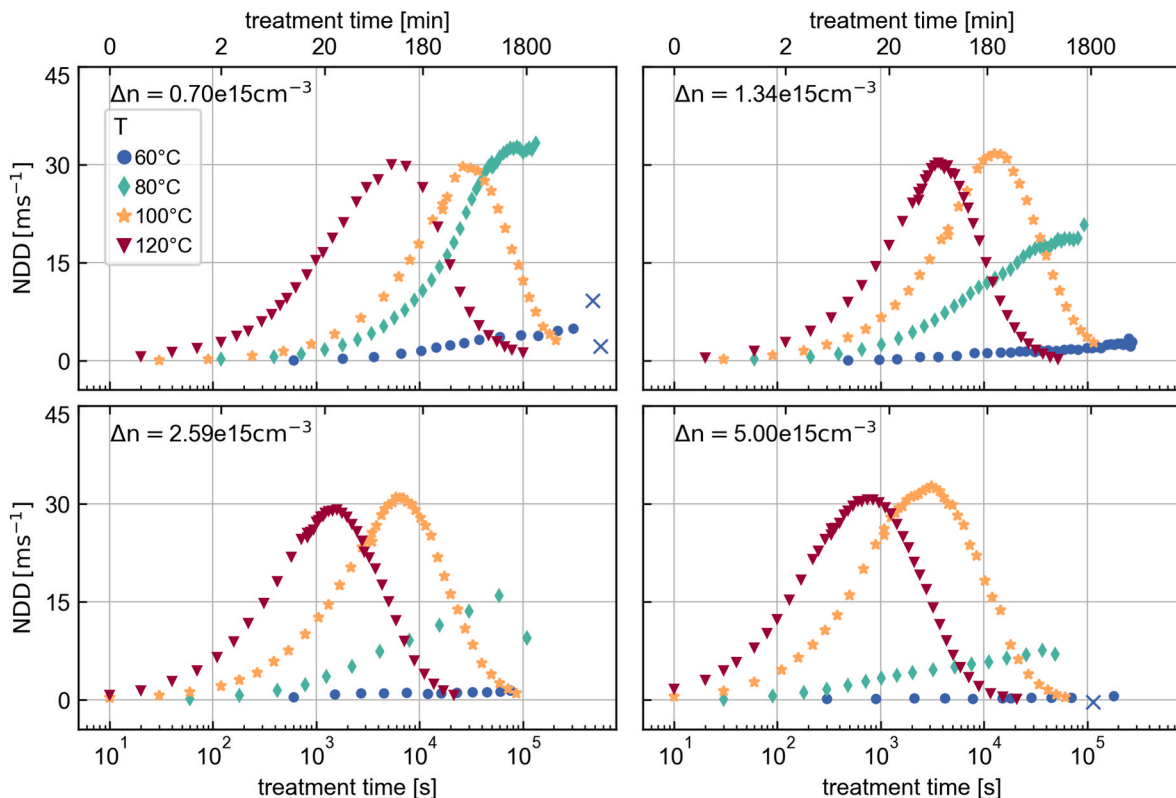


Fig. 1. NDD as a function of treatment time for different injection levels (panels) and the different temperatures (color coded).

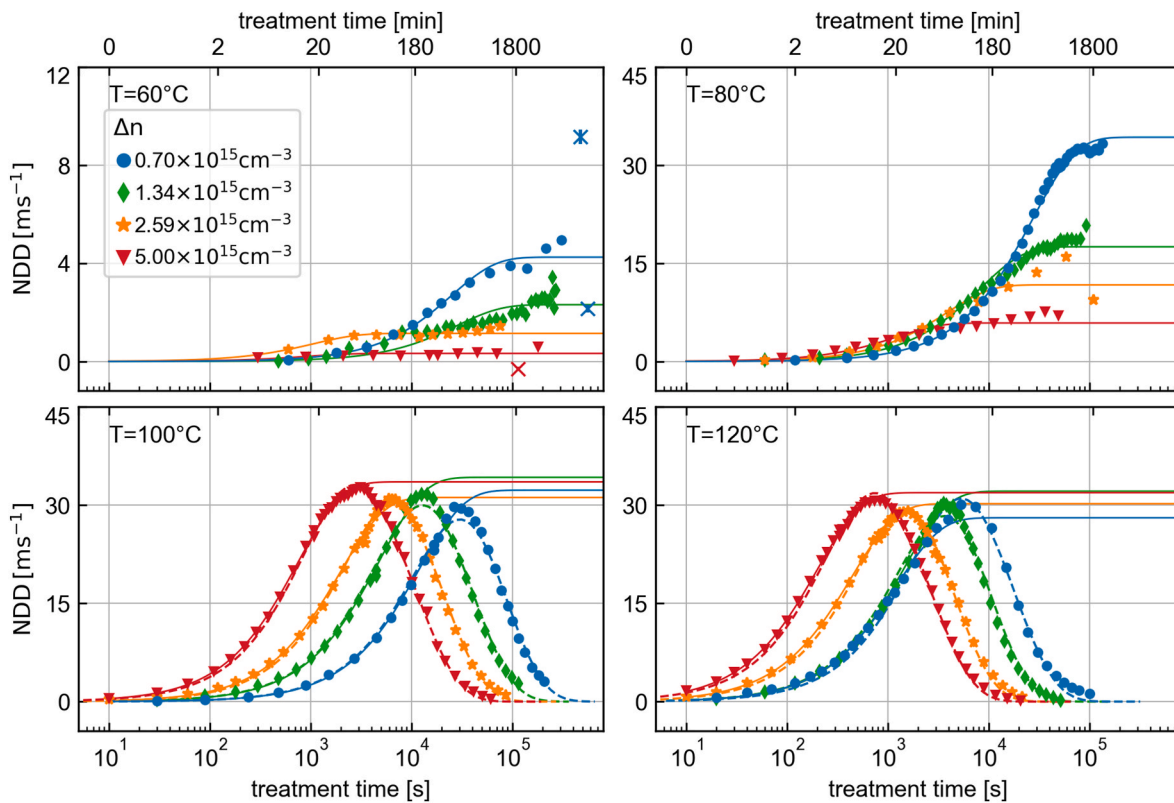


Fig. 2. NDD as a function of treatment time for different temperatures (panels) and the different injection levels (color coded). Solid and dashed lines are fits to equations (5) and (7), respectively. Values marked as crosses are excluded from fits.

different curves to intersect, leading to an overall more complex picture. In addition, the NDD begins to fluctuate as the timesteps between measurements get larger (e.g. 60 °C, 0. $7 \times 10^{15} \text{cm}^{-3}$). This is only partially due to the overall lower degradation extent (note the scale for 60 °C). More importantly, it is inherently difficult to maintain constant injection at low temperature, as will be explained in the next section.

4.2. Discussion of temperature and injection screening

The primary influence on both extent and speed of LeTID is the temperature, while the injection takes a secondary but still very important role. At lower temperatures, the most prominent feature is the lower LeTID extent with respect to the NDD values reached at 100 °C and 120 °C. The measured NDD at 60 and 80 °C depends counterintuitively on the injection level, i.e. a higher injection leads to a lower overall degradation. We attribute this behavior to TR suppressing the effective degradation in Si:Ga even at elevated temperatures as high as 80 °C. Notably, the Si:B reference samples do not show increased LeTID suppression with increasing injection level despite the equivalent processing (see Supplementary Fig. 3). We conclude that (i) the LeTID resilience often associated with Gallium doping arises from a stronger tendency towards TR as found in Si:B and (ii) the dopant atom influences at least one of the reactions between states A and B, i.e. degradation and/or TR.

The injection dependence of the TR-induced suppression of LeTID in Si:Ga results from the competition between degradation and TR. The contrary processes of defect formation and precursor reformation shift the system to a balanced state with an equilibrium population of defects given by $\text{NDD}_{\text{eq}} = \text{NDD}|_{t \rightarrow \infty} = \frac{A_0 k_{\text{AB}}}{k_{\text{AB}} + k_{\text{BA}}}$ (from equation (6)). Since both transition coefficients have a different injection and temperature dependence, the equilibrium defect density must also be influenced by both temperature and injection. The trends we observe for NDD_{eq} are thereby in accordance with the injection dependence of the transition

coefficients as presented in section 4.3: TR scales approximately quadratic with injection while degradation has a roughly linear dependence. Furthermore, the temperature activation of TR is reported to be much weaker than that of the degradation transition [39]. Hence, the LeTID suppression is only present for a sufficiently low temperature, i.e. in the upper panels of Fig. 2, and more effective for higher injections. Note that a similar LeTID suppression is expected to occur for Si:B as well [39,52], but only at much lower temperatures.

At 60 °C, which is the closest to field conditions, the injection significantly determines the effective LeTID kinetics with an almost complete degradation suppression for $\Delta n = 5 \times 10^{15} \text{cm}^{-3}$. This explains reports of Cz-Si:Ga-samples that were stable at one sun equivalent illumination, while showing significant LeTID degradation at 0.15 suns equivalent illumination [5]. The one sun equivalent illumination activated TR such that no significant formation of LeTID defects is observed. Our findings also highlight that the tendency to TR in Si:Ga is not equivalent to a general LeTID immunity, but rather an increased resistance at specific conditions, i.e. low temperature and high injection.

A second effect of strong TR is apparent from the fluctuations in the NDD-values once the timesteps between measurements and thus generation adjustments become larger ($\sim 10^5 \text{s}$). The origin of the fluctuations is a positive feedback loop induced by TR that drives the injection away from the targeted values, compromising the experimental approach: If the generation is regulated after a measurement point such that the injection is slightly lower than the target Δn_t , the balance between degradation and TR tips in favor of faster formation of defects. The effective lifetime decreases and the NDD shifts to slightly higher values. The resulting decrease of injection closes the positive feedback loop. In this scenario, the NDD continues to drive towards higher values until the next measurement is taken and the injection can be reset to the target value by increasing the illumination. However, the systems' defect density is at this point already much higher than the equilibrium value $\text{NDD}_{\text{eq}}(\Delta n) \gg \text{NDD}_{\text{eq}}(\Delta n_t)$. Strong and self-reinforcing TR then

leads to a fast reduction in NDD that can easily undershoot the equilibrium value for the targeted injection since the feedback loop also applies in reverse direction. This phenomenon could be avoided by measuring lifetime in-situ and adapting the generation at much smaller time steps. The appearance of the fluctuations towards both higher and lower NDD values (see for example the last two data points at 60 °C, $0.7 \times 10^{15} \text{cm}^{-3}$) cannot be described by regeneration and thus confirms TR as the cause of the suppression of LeTID extent at low values for low temperatures.

While TR determines the LeTID kinetics at lower temperatures, it appears to be insignificant at 100 °C and 120 °C. Here, a typical LeTID cycle consisting of degradation followed by regeneration is observed. This motivates the approximation $k_{BA} \approx 0$ at 100 and 120 °C for the following discussion. Our data suggests that the time after which the degradation maximum is reached is reduced for higher temperatures and injections, while the value of NDD remains roughly invariant. These quantities follow within the three-state-model as

$$t_{\max} = \frac{\ln(k_{AB}/k_{BC})}{k_{AB} - k_{BC}} \quad (8)$$

and

$$B(t_{\max}) = \frac{k_{AB}A_0}{k_{AB} - k_{BC}} \left(\frac{k_{AB}^{-k_{BC}}}{k_{BC}^{k_{AB}-k_{BC}}} - \frac{k_{AB}^{-k_{AB}}}{k_{BC}^{k_{AB}-k_{BC}}} \right), \quad (9)$$

respectively (from the derivative of equation (7)). This shows that the maximum defect density is a complex function of both the degradation and regeneration transition coefficients. Due to their dependence on temperature and injection, the measured maximum in NDD is thus a priori expected to show a corresponding dependence. In contrast, our data shows similar levels of NDD_{\max} over a wide range of temperatures and injections. We conclude that the activation energy and the injection exponent (as defined in equation (4)) for the degradation and regeneration transition are at least similar, i.e. $E_a^{AB} \approx E_a^{BC}$ and $x_{AB} \approx x_{BC}$. In this scenario, the temperature and injection dependence cancel from each individual term of equation (9) and the degradation maximum is only determined by the two attempt frequencies associated with the respective transitions and the precursor density A_0 . The latter is expected to be similar for the whole sample set due to the equal processing.

Note that t_{\max} would still feature an injection and temperature dependence, specifically of the form

$$t_{\max} = \frac{\ln(\nu_{AB}/\nu_{BC})}{\nu_{AB} - \nu_{BC}} \left(\frac{\Delta n}{\Delta n_0} \right)^{-x_{AB}} \exp\left(\frac{E_a^{AB}}{kT}\right). \quad (10)$$

We probe the injection dependence of this proposed equation by plotting t_{\max} as a function of injection levels and indeed find good agreement with an injection exponent of $x_{AB} \approx x_{BA}$ close to unity (see [Supplementary Fig. 4](#)). Our findings thus strongly suggest that degradation and regeneration are limited by the same or at least a similar physical process.

4.3. Transition rate coefficients

We extract the rate coefficients of the LeTID transitions from the NDD-data by utilizing the three-state-model. The rise-to-maximum fit following equation (5) (solid lines in [Fig. 2](#)) considers only the rising edge of a LeTID cycle and yields an effective transition rate coefficient $k_{\text{eff}} = k_{AB} + k_{BA}$. For 100 °C and 120 °C, this method of analysis can be improved upon by specifying $k_{BA} \approx 0$ and fitting equation (7) to the full LeTID cycle (dashed lines in [Fig. 2](#)). For 60 °C and 80 °C, the interplay between TR and degradation is dominating the kinetics. The rise-to-maximum fits can be further analyzed by applying equation (6) which splits the effective transition coefficient into its components $k_{\text{eff}} = k_{AB} + k_{BA}$.

Utilizing equation (6) as opposed to (5) requires knowledge of the

LeTID precursor density A_0 , which is expected to scale with the bulk density of molecular hydrogen. The equal processing of all our samples suggests equal hydrogen content and consequently that the whole dataset should be well described with a single A_0 . We find A_0 as a global optimization parameter from fits to the curves where $k_{BA} \approx 0$, i.e. 100 °C and 120 °C. [Supplementary Fig. 5](#) shows a clear minimum at $A_0 \approx 43 \text{ms}^{-1}$ in the global loss function calculated via the individual fit residuals. The agreement between the NDD data and the dashed lines in [Fig. 2](#), where $A_0 \approx 43 \text{ms}^{-1}$ was set as an input, further justifies our assumption of a global A_0 . The minor deviations that are apparent could stem from sample-to-sample variations in the hydrogen content that can appear despite the equal processing [21]. To illustrate the disadvantages of an analysis focusing on effective transitions, we also extract k_{eff} via equation (5) for each curve, taking only the rising edge even if regeneration was measured.

The logarithm of the effective rate coefficients is depicted in [Fig. 3a](#) as a function of inverse temperature. In this Arrhenius representation, the coefficients for 80 °C, 100 °C and 120 °C lie approximately on a straight line for all injections. The rate coefficients extracted at 60 °C do not fit this trend and are instead larger than those extracted at 80 °C (with one outlier for $\Delta n = 1.34 \times 10^{15} \text{cm}^{-3}$). A similar saturation of the effective transition rate coefficient for low temperatures was previously observed by Winter et al. for both Si:Ga and Si:B, but no explanation could be offered besides experimental uncertainty [26,41]. Now, we can explain such a behaviour: Its origin in our dataset is the onset of TR at lower temperatures. As the effective rate coefficient k_{eff} is then the sum of the individual ones ($k_{\text{eff}} = k_{AB} + k_{BA}$), the data in [Fig. 3a](#) is expected to reflect both the Arrhenius-behavior associated with the degradation transition and the increase of k_{BA} with lower temperature associated with TR [39]. At high temperatures, the values of k_{eff} suffer from the unjustified fit-assumption of negligible k_{BC} . The resulting effective activation energy (from fits to equation (4)) averaged over all injection levels is with $E_a^{\text{eff}} = (0.65 \pm 0.09) \text{eV}$ nonetheless consistent with the value reported by Winter et al. [41].

[Fig. 3b](#) shows the pure degradation coefficients k_{AB} as determined via equations (6) and (7). The influence of TR and regeneration is now accounted for where appropriate resulting in an Arrhenius behavior for the complete temperature range. The value of the activation energy averaged over all injections increases to $E_a^{AB} = (0.86 \pm 0.08) \text{eV}$ (see also [Fig. 4](#)). This – more trustworthy – value agrees closely with the one recently determined by Zerfaß et al. [19]. Notably, the authors avoided all pitfalls that can skew the value of activation energy, i.e. they probed the LeTID cycle at constant injection condition, fitted the full LeTID cycle and studied a temperature range where TR is not expected to be important. We recommend a similar procedure for future studies on the topic and stress that E_a^{AB} as opposed to E_a^{eff} resembles the rate-limiting energy barrier in the degradation reaction.

The injection exponents x_{eff} , x_{AB} , x_{BA} and x_{BC} were extracted via a fit to equation (4) from the effective-, degradation-, TR-, and regeneration rate coefficients, respectively. The transition coefficients and fits can be found in [Supplementary Fig. 6](#), while the values for the injection exponent are summarized in [Fig. 4](#).

The effective injection exponent obtained via k_{eff} lies between one and two. In contrast, the injection exponent for the pure degradation transition scatters around one. This is in line with the value determined from the time required to reach the degradation maximum t_{\max} ([Supplementary Fig. 4](#)). This alternative determination rests on the assumption that the activation energy and injection exponent of the degradation and regeneration transition are similar. This hypothesis is now also supported quantitatively since the x_{BC} extracted via the rate coefficients is close to unity as well. For TR, the qualitatively observed increase of LeTID suppression with higher injection implies a higher injection exponent x_{BA} . And indeed, the value lies at two meaning all injections exponents extracted here for Si:Ga are in agreement with results established for Si:B [14,39]. Since the injection exponent can also

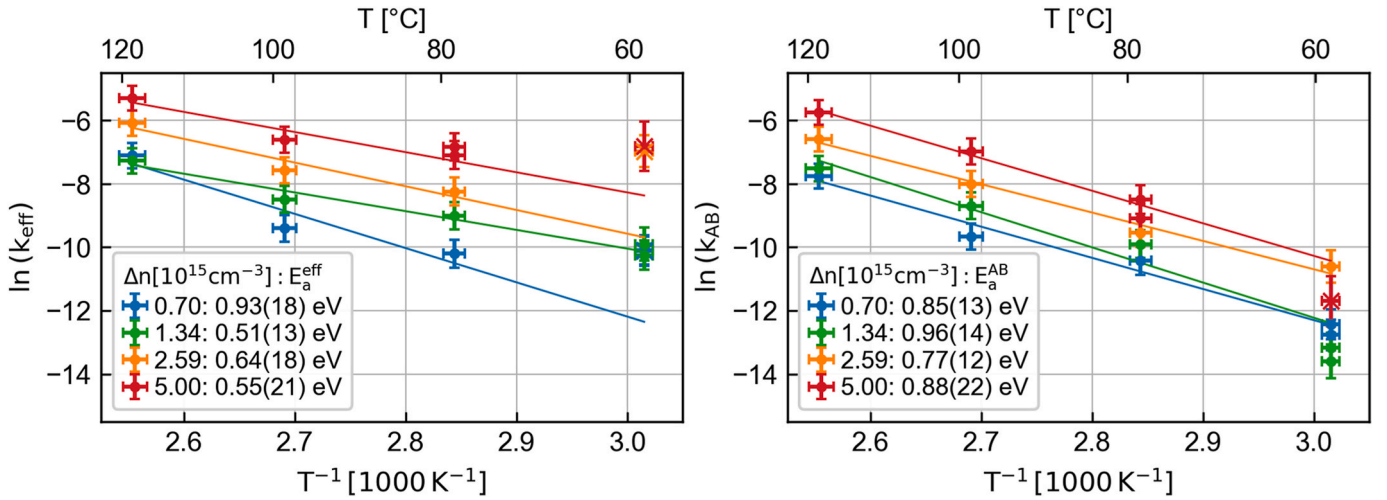


Fig. 3. Logarithm of effective (a) and degradation (b) rate coefficients determined from fits to NDD-data as a function of the inverse temperature. Arrhenius behavior is only seen throughout the whole temperature range if TR is accounted for, i.e. in the right.

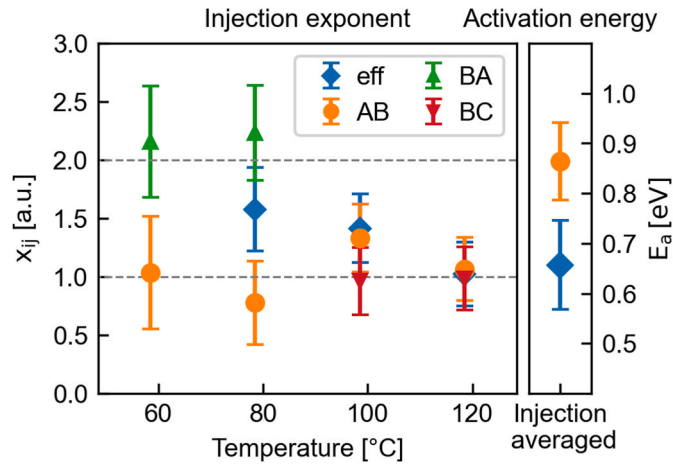


Fig. 4. Injection exponents and activation energy as determined from rate coefficients. Analyzing the effective rate coefficients underestimates the pure degradation activation energy and yields non-integer injection exponents. This can be overcome by evaluating the rate coefficients corresponding to the transitions separately.

be seen as the stoichiometric factor of an underlying transition reaction, we can conclude the degradation and regeneration transition are both rate-limited by a process requiring one excess charge carrier, whereas it is two for the TR reaction. In summary, our method of analysis with the inclusion of TR leads to a consistent set of physically meaningful parameters.

Besides enhancing the understanding of LeTID on the atomic scale, these results also serve as direct input parameters for kinetic models that aim to forecast the evolution of modules in the field [53]. Our method of analysis leads to a systematic improvement on the accuracy of the activation energy and injection exponents. The values we advise to use for modelling of Si:Ga are summarized in Table 1.

Table 1
Kinetic parameters of the LeTID transition coefficients for equation (4).

Parameter	Transition		
	AB	BC	BA
E_a^{ij} [eV]	0.86	$\approx E_a^{AB}$	–
x_{ij}	1	1	2

4.4. Implications for test sequences

Fig. 5 maps the information gathered from the temperature and injection screening onto contour plots that show the maximum degradation extent (a) in comparison with the effective rate coefficient (b). The latter is the appropriate quantity to describe the apparent rate of NDD-increase. We also add the half life $t_{1/2} = \ln(2)k_{\text{eff}}^{-1}$ to some contour lines but stress that the time required for testing is on average about four times larger (determined from t_{max} for 100 °C and 120 °C). The trends apparent in the figure have been discussed in detail before, hence this section will focus on their implications for test sequences.

The left figure can easily be divided into a region where TR significantly reduces degradation (below blue contour line) and one where degradation and regeneration determine the kinetics, yielding a plateau of similar degradation extent (above blue contour line). Importantly, the plateau extends at low injections towards low temperatures, indicating a significant degradation can occur when moving towards field conditions (FC, see Supplementary Fig. 7). The effective rate coefficient is at this point minimal, meaning a “slow burn” can unfold. This poses a major risk for photovoltaic installations as the degradation would only be noticed long after modules have been installed in the field.

Fortunately, the potential degradation at field conditions can be probed at any point on the plateau. Going along the arrows of Fig. 5 towards proposed test conditions (TC) allows for strongly accelerated testing with an expected equal outcome in terms of maximum LeTID extent. Within the probed parameter space, we attain two orders of magnitude acceleration reducing the time required to reach the LeTID maximum to about 15 min. Probing at constant injection as opposed to constant illumination thereby ensures that lifetime degradation and the corresponding reduction of minority charge carrier density do not decrease the transition rate throughout an experiment.

It is expected that the test duration can be further reduced by increasing the temperature and injection to more extreme values. However, care should be taken for either parameter. Increasing the injection leads to stronger TR which could limit the probed degradation extent. This is directly evident in our data, where a test at 80 °C and $5 \times 10^{15} \text{ cm}^{-3}$ would suggest less LeTID susceptibility than the seemingly less severe at 80 °C and $0.7 \times 10^{15} \text{ cm}^{-3}$. A higher temperature could lead to a replenishment of the LeTID precursors [54,55] or induce non-LeTID-related processes such as surface degradation. It should also be noted that modules cannot be heated to temperatures higher than 85 °C without risking damage to their components.

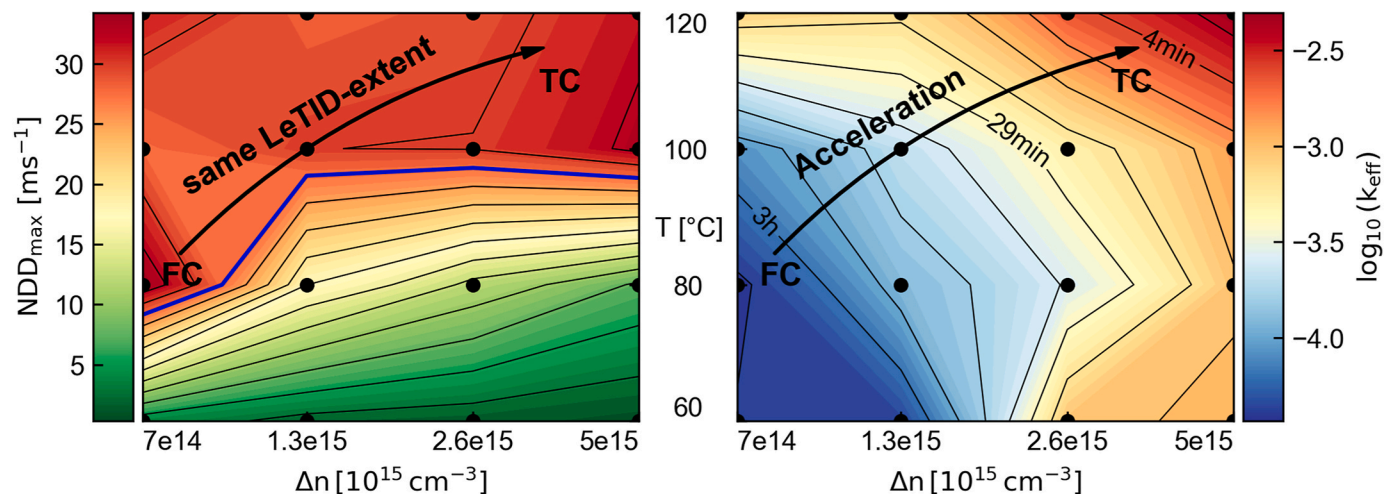


Fig. 5. NDD_{max} and logarithm of effective transition coefficient as a function of both injection and temperature. The plateau above the blue line in the left figure enables testing the LeTID extent at field conditions (FC) at proposed testing conditions (TC) with an acceleration factor of 100.

5. Summary and conclusion

We investigated the LeTID kinetics in Si:Ga and found clear evidence that the balance between degradation and temporary recovery (TR) is shifted towards TR when compared to Si:B. This suggests that the dopant atom is involved in at least one of the two competing reactions. The resulting TR-induced suppression of the degradation extent at temperatures up to 80 °C is responsible for the LeTID resistance often ascribed to Gallium-doping. However, degradation can still appear at low injection conditions, meaning Gallium-doping does not create an inherent LeTID immunity. Whether LeTID occurs in Gallium-doped photovoltaics will be decided by several factors ranging from the hydrogen content in the silicon bulk, through the cell design determining the effective carrier lifetime, to the conditions to which the finished module is exposed to.

We showed that extracting kinetic parameters from LeTID experiments and NDD curves requires careful design of experiment. In particular, it is advised to (i) measure at constant charge carrier injection, (ii) probe and fit the full LeTID cycle including regeneration and (iii) either account for TR or avoid it by measuring at temperatures where its role is minor. Otherwise, measured NDD-curves suggest more complex transition-behavior than actually present, the degradation activation energy is underestimated and the injection exponents take non-integer values.

We find that the LeTID extent is independent of both temperature and injection when TR is negligible and conclude that regeneration and degradation share similar kinetics. This hypothesis is supported by the quantitative analysis of rate coefficients that results in injection exponents of $x_{AB} \approx x_{BC} \approx 1$ and $x_{BA} \approx 2$. These values suggest one electron is required for the rate-limiting reaction of degradation and regeneration, whereas two are required for TR. The degradation activation energy was determined as $E_a^{AB} = (0.86 \pm 0.08)$ eV. With the approximation $E_a^{BC} \approx E_a^{AB}$, we supply an almost complete set of kinetic parameters required for yield modelling of Si:Ga based photovoltaic devices. The exact temperature dependence of TR remains to be quantitatively described.

Finally, we demonstrate that the correct test strategy can reproduce the potential degradation extent possible at field conditions at a 100-fold accelerated rate in Si:Ga. Key points for reliable and fast testing are to probe at high temperature and high but constant injection while remaining within a range where the degradation extent is governed by the interplay between LeTID-degradation and -regeneration only. The acceleration factor can likely further be increased for solar cells and their precursors, whereas the potential is limited for modules. Hence, the bulk of LeTID testing must already occur on cell or wafer level.

Funding sources

The authors acknowledge the financial support by the Federal Ministry for Economic Affairs and Climate Action of Germany in the project GagarIn (funding codes 03EE1133A and 03EE1133B). The work of Fabian T. Thome was supported by the scholarship of the German Federal Environmental Foundation (“Deutsche Bundesstiftung Umwelt”).

CRediT authorship contribution statement

Fabian T. Thome: Writing – original draft, Visualization, Validation, Methodology, Investigation, Funding acquisition, Formal analysis, Data curation, Conceptualization. **Cem Yilmaz:** Formal analysis, Data curation. **Wolfram Kwapil:** Writing – review & editing, Supervision, Project administration, Funding acquisition, Conceptualization. **Florian Schindler:** Writing – review & editing, Supervision, Project administration, Funding acquisition. **Martin C. Schubert:** Writing – review & editing, Project administration, Funding acquisition.

Declaration of competing interest

The authors declare that they have no known competing financial interests or personal relationships that could have appeared to influence the work reported in this paper.

Data availability

Data will be made available on request.

Appendix A. Supplementary data

Supplementary data to this article can be found online at <https://doi.org/10.1016/j.solmat.2024.112986>.

References

- [1] M. Fischer, M. Woodhouse, S. Herritsch, J. Trube, *International Technology Roadmap for Photovoltaic (ITRPV)*, VDMA e. V., Frankfurt am Main, Germany, 2023.
- [2] Gallium-doped Monocrystalline Silicon Fully Solves the Problem of a PERC Module's LID, LONGi News, 2020. <https://www.longi.com/en/news/6880/>. (Accessed 29 January 2024).
- [3] S.W. Glunz, S. Rein, J. Knobloch, W. Wettling, T. Abe, Comparison of boron- and gallium-doped p-type Czochralski silicon for photovoltaic application, *Prog. Photovolt. Res. Appl.* 7 (1999) 463–469, [https://doi.org/10.1002/\(SICI\)1099-159X\(199911/12\)7:6<463::AID-PIP293>3.0.CO;2-H](https://doi.org/10.1002/(SICI)1099-159X(199911/12)7:6<463::AID-PIP293>3.0.CO;2-H).

- [4] F. Kersten, P. Engelhart, H.-C. Ploigt, A. Stekolnikov, T. Lindner, F. Stenzel, M. Bartzsch, A. Szpeth, K. Petter, J. Heitmann, J.W. Müller, Degradation of multicrystalline silicon solar cells and modules after illumination at elevated temperature, *Sol. Energy Mater. Sol. Cells* 142 (2015) 83–86, <https://doi.org/10.1016/j.solmat.2015.06.015>.
- [5] W. Kwapil, J. Dalke, R. Post, T. Niewelt, Influence of dopant elements on degradation phenomena in B- and Ga-doped Czochralski-grown silicon, *Sol. RRL* 5 (2021) 2100147, <https://doi.org/10.1002/solr.202100147>.
- [6] J.M. Fritz, A. Zuschlag, D. Skorka, A. Schmid, G. Hahn, Temperature dependent degradation and regeneration of differently doped mc-Si materials, *Energy Proc.* 124 (2017) 718–725, <https://doi.org/10.1016/j.egypro.2017.09.085>.
- [7] K. Ramspeck, S. Zimmermann, H. Nagel, A. Metz, Y. Gassenbauer, B. Birkmann, A. Seidl, Light induced degradation of rear passivated mc-Si solar cells, in: 27th Eur. Photovolt. Sol. Energy Conf., Exhib., WIP, 2012, pp. 861–865, <https://doi.org/10.4229/27THEUPVSEC2012-2DO.3.4>.
- [8] C.E. Chan, D.N.R. Payne, B.J. Hallam, M.D. Abbott, T.H. Fung, A.M. Wenham, B. S. Tjahjono, S.R. Wenham, Rapid stabilization of high-performance multicrystalline P-type silicon PERC cells, *IEEE J. Photovolt.* 6 (2016) 1473–1479, <https://doi.org/10.1109/JPHOTOV.2016.2606704>.
- [9] D. Bredemeier, D. Walter, S. Herlufsen, J. Schmidt, Lifetime degradation and regeneration in multicrystalline silicon under illumination at elevated temperature, *AIP Adv.* 6 (2016) 035119, <https://doi.org/10.1063/1.4944839>.
- [10] W. Kwapil, T. Niewelt, M.C. Schubert, Kinetics of carrier-induced degradation at elevated temperature in multicrystalline silicon solar cells, *Sol. Energy Mater. Sol. Cells* 173 (2017) 80–84, <https://doi.org/10.1016/j.solmat.2017.05.066>.
- [11] D. Chen, M. Kim, B.V. Stefani, B.J. Hallam, M.D. Abbott, C.E. Chan, R. Chen, D.N. R. Payne, N. Nampalli, A. Ciesla, T.H. Fung, K. Kim, S.R. Wenham, Evidence of an identical firing-activated carrier-induced defect in monocrystalline and multicrystalline silicon, *Sol. Energy Mater. Sol. Cells* 172 (2017) 293–300, <https://doi.org/10.1016/j.solmat.2017.08.003>.
- [12] F. Fertig, R. Lantzsich, A. Mohr, M. Schaper, M. Bartzsch, D. Wissen, F. Kersten, A. Mette, S. Peters, A. Eidner, J. Cieslak, K. Duncker, M. Junghänel, E. Jarzembowski, M. Kauer, B. Faulwetter-Quandt, D. Meißner, B. Reiche, S. Geißler, S. Hörnlein, C. Klenke, L. Niebergall, A. Schönmann, A. Wehrauch, F. Stenzel, A. Hofmann, T. Rudolph, A. Schwabedissen, M. Gundermann, M. Fischer, J.W. Müller, D.J.W. Jeong, Mass production of p-type Cz silicon solar cells approaching average stable conversion efficiencies of 22, *Energy Proc.* 124 (2017) 338–345, <https://doi.org/10.1016/j.egypro.2017.09.308>.
- [13] D. Sperber, F. Furtwängler, A. Herguth, G. Hahn, On the stability of dielectric passivation layers under illumination and temperature treatments, in: 32nd Eur. Photovolt. Sol. Energy Conf., Exhib., WIP, 2016, pp. 523–526, <https://doi.org/10.4229/EUPVSEC20162016-2DO.3.4>.
- [14] T. Niewelt, M. Selinger, N.E. Grant, W. Kwapil, J.D. Murphy, M.C. Schubert, Light-induced activation and deactivation of bulk defects in boron-doped float-zone silicon, *J. Appl. Phys.* 121 (2017) 185702, <https://doi.org/10.1063/1.4983024>.
- [15] T. Niewelt, F. Schindler, W. Kwapil, R. Eberle, J. Schön, M.C. Schubert, Understanding the light-induced degradation at elevated temperatures: similarities between multicrystalline and floatzone p-type silicon, *Prog. Photovolt. Res. Appl.* 26 (2018) 533–542, <https://doi.org/10.1002/ppp.2954>.
- [16] F. Kersten, F. Fertig, K. Petter, B. Klöter, E. Herzog, M.B. Strobel, J. Heitmann, J. W. Müller, System performance loss due to LeTID, *Energy Proc.* 124 (2017) 540–546, <https://doi.org/10.1016/j.egypro.2017.09.260>.
- [17] R. Eberle, W. Kwapil, F. Schindler, M.C. Schubert, S.W. Glunz, Impact of the firing temperature profile on light induced degradation of multicrystalline silicon, *Phys. Status Solidi RRL* 10 (2016) 861–865, <https://doi.org/10.1002/pssr.201600272>.
- [18] J. Schmidt, D. Bredemeier, D.C. Walter, On the defect physics behind light and elevated temperature-induced degradation (LeTID) of multicrystalline silicon solar cells, *IEEE J. Photovolt.* 9 (2019) 1497–1503, <https://doi.org/10.1109/JPHOTOV.2019.2937223>.
- [19] R. Zerfaß, J. Simon, A. Herguth, G. Hahn, Impact of hydrogen in Ga-doped silicon on maximum LeTID defect density, *Sol. RRL* (2023) 2300501, <https://doi.org/10.1002/solr.202300501>.
- [20] C. Vargas, K. Kim, G. Coletti, D. Payne, C. Chan, S. Wenham, Z. Hameiri, Carrier-induced degradation in multicrystalline silicon: dependence on the silicon nitride passivation layer and hydrogen released during firing, *IEEE J. Photovolt.* 8 (2018) 413–420, <https://doi.org/10.1109/JPHOTOV.2017.2783851>.
- [21] J. Simon, R. Fischer-Süßlin, R. Zerfaß, L. Kutschera, P. Dufke, A. Herguth, S. Roder, G. Hahn, Correlation study between LeTID defect density, hydrogen and firing profile in Ga-doped crystalline silicon, *Sol. Energy Mater. Sol. Cells* 260 (2023) 112456, <https://doi.org/10.1016/j.solmat.2023.112456>.
- [22] B. Hammann, N. Assmann, P.M. Weiser, W. Kwapil, T. Niewelt, F. Schindler, R. Sondenå, E.V. Monakhov, M.C. Schubert, The impact of different hydrogen configurations on light- and elevated-temperature- induced degradation, *IEEE J. Photovolt.* 13 (2023) 224–235, <https://doi.org/10.1109/JPHOTOV.2023.3236185>.
- [23] F. Maischner, S. Maus, J. Greulich, S. Lohmüller, E. Lohmüller, P. Saint-Cast, D. Ourinson, H. Vahlman, K. Hergert, S. Riepe, S. Glunz, S. Rein, LeTID mitigation via an adapted firing process in p-type PERC cells from SMART cast-monocrystalline, Czochralski and high-performance multicrystalline silicon, *Prog. Photovolt. Res. Appl.* 30 (2022) 123–131, <https://doi.org/10.1002/ppp.3467>.
- [24] F. Maischner, J.M. Greulich, W. Kwapil, D. Ourinson, S.W. Glunz, S. Rein, LeTID mitigation via an adapted firing process in p-type PERC cells from gallium-doped Czochralski silicon, *Sol. Energy Mater. Sol. Cells* 262 (2023) 112529, <https://doi.org/10.1016/j.solmat.2023.112529>.
- [25] B. Hammann, N. Assmann, J. Schön, W. Kwapil, F. Schindler, S. Roder, E. V. Monakhov, M.C. Schubert, Understanding the impact of the cooling ramp of the fast-firing process on light- and elevated-temperature-induced degradation, *Sol. Energy Mater. Sol. Cells* 259 (2023) 112462, <https://doi.org/10.1016/j.solmat.2023.112462>.
- [26] M. Winter, D.C. Walter, J. Schmidt, Impact of fast-firing conditions on light- and elevated-temperature-induced degradation (LeTID) in Ga-doped Cz-Si, *IEEE J. Photovolt.* (2023) 1–9, <https://doi.org/10.1109/JPHOTOV.2023.3304118>.
- [27] D. Bredemeier, D.C. Walter, J. Schmidt, Possible candidates for impurities in mc-Si wafers responsible for light-induced lifetime degradation and regeneration, *Sol. RRL* 2 (2018) 1700159, <https://doi.org/10.1002/solr.201700159>.
- [28] U. Varshney, M. Kim, M.U. Khan, P. Hamer, C. Chan, M. Abbott, B. Hoex, Impact of substrate thickness on the degradation in multicrystalline silicon, *IEEE J. Photovolt.* 11 (2021) 65–72, <https://doi.org/10.1109/JPHOTOV.2020.3038412>.
- [29] U. Varshney, M. Abbott, A. Ciesla, D. Chen, S. Liu, C. Sen, M. Kim, S. Wenham, B. Hoex, C. Chan, Evaluating the impact of SiN_x thickness on lifetime degradation in silicon, *IEEE J. Photovolt.* 9 (2019) 601–607, <https://doi.org/10.1109/JPHOTOV.2019.2896671>.
- [30] D. Bredemeier, D.C. Walter, R. Heller, J. Schmidt, Impact of hydrogen-rich silicon nitride material properties on light-induced lifetime degradation in multicrystalline silicon, *Phys. Status Solidi RRL* 13 (2019) 1900201, <https://doi.org/10.1002/pssr.201900201>.
- [31] L. Helmich, D.C. Walter, D. Bredemeier, J. Schmidt, Atomic-layer-deposited Al₂O₃ as effective barrier against the diffusion of hydrogen from SiN_x/H layers into crystalline silicon during rapid thermal annealing, *Phys. Status Solidi RRL* 14 (2020) 2000367, <https://doi.org/10.1002/pssr.202000367>.
- [32] U. Varshney, B. Hallam, P. Hamer, A. Ciesla, D. Chen, S. Liu, C. Sen, A. Samadi, M. Abbott, C. Chan, B. Hoex, Controlling light- and elevated-temperature-induced degradation with thin film barrier layers, *IEEE J. Photovolt.* 10 (2020) 19–27, <https://doi.org/10.1109/JPHOTOV.2019.2945199>.
- [33] A. Schmid, C. Fischer, D. Skorka, A. Herguth, C. Winter, A. Zuschlag, G. Hahn, On the role of AlO_x thickness in AlO_x/SiN_x/H layer stacks regarding light- and elevated temperature-induced degradation and hydrogen diffusion in c-Si, *IEEE J. Photovolt.* 11 (2021) 967–973, <https://doi.org/10.1109/JPHOTOV.2021.3075850>.
- [34] F. Maischner, W. Kwapil, J.M. Greulich, Y. Jung, H. Höfler, P. Saint-Cast, M. C. Schubert, S. Rein, S.W. Glunz, Process influences on LeTID in Ga-doped silicon, *Sol. Energy Mater. Sol. Cells* 260 (2023) 112451, <https://doi.org/10.1016/j.solmat.2023.112451>.
- [35] T. Niewelt, F. Maischner, W. Kwapil, E. Khorani, S.L. Pain, Y. Jung, E.C.B. Hopkins, M. Frosch, P.P. Altermatt, H. Guo, Y.C. Wang, N.E. Grant, J.D. Murphy, Stability of industrial gallium-doped Czochralski silicon PERC cells and wafers, *Sol. Energy Mater. Sol. Cells* 266 (2024) 112645, <https://doi.org/10.1016/j.solmat.2023.112645>.
- [36] J.-I. Polzin, B. Hammann, T. Niewelt, W. Kwapil, M. Hermler, F. Feldmann, Thermal activation of hydrogen for defect passivation in poly-Si based passivating contacts, *Sol. Energy Mater. Sol. Cells* 230 (2021) 111267, <https://doi.org/10.1016/j.solmat.2021.111267>.
- [37] C. Chen, H. Wang, J. Wang, J. Lv, H. Yang, Performance degradation of commercial Ga-doped passivated emitter and rear cell solar modules in the field, *Prog. Photovolt. Res. Appl.* 30 (2022) 300–309, <https://doi.org/10.1002/ppp.3512>.
- [38] N.E. Grant, J.R. Scowcroft, A.I. Pointon, M. Al-Amin, P.P. Altermatt, J.D. Murphy, Lifetime instabilities in gallium doped monocrystalline PERC silicon solar cells, *Sol. Energy Mater. Sol. Cells* 206 (2020) 110299, <https://doi.org/10.1016/j.solmat.2019.110299>.
- [39] W. Kwapil, J. Schön, T. Niewelt, M.C. Schubert, Temporary recovery of the defect responsible for light- and elevated temperature-induced degradation: insights into the physical mechanisms behind LeTID, *IEEE J. Photovolt.* 10 (2020) 1591–1603, <https://doi.org/10.1109/JPHOTOV.2020.3025240>.
- [40] S. Liu, C. Chan, D. Chen, M. Kim, C. Sen, U. Varshney, B. Hallam, M. Abbott, S. Wenham, D. Payne, Investigation of temperature and illumination dependencies of carrier-induced degradation in p-type multi-crystalline silicon, in: *SiliconPV 2018 8th Int. Conf. Cryst. Silicon Photovolt.*, AIP, 2018, <https://doi.org/10.1063/1.5049333>, 130014-1-130014-8.
- [41] M. Winter, D. Walter, J. Schmidt, Carrier lifetime degradation and regeneration in gallium- and boron-doped monocrystalline silicon materials, *IEEE J. Photovolt.* 11 (2021) 866–872, <https://doi.org/10.1109/JPHOTOV.2021.3070474>.
- [42] S. Jafari, Z. Hameiri, Investigation of light-induced degradation in Ga- and indoped Cz silicon, in: 2021 IEEE 48th Photovolt. Spec. Conf. PVSC, 2021, pp. 814–817, <https://doi.org/10.1109/PVSC43889.2021.9518574>.
- [43] D. Lin, Z. Hu, L. Song, D. Yang, X. Yu, Investigation on the light and elevated temperature induced degradation of gallium-doped Cz-Si, *Sol. Energy* 225 (2021) 407–411, <https://doi.org/10.1016/j.solener.2021.07.023>.
- [44] S. Rein, T. Rehr, W. Warta, S.W. Glunz, Lifetime spectroscopy for defect characterization: systematic analysis of the possibilities and restrictions, *J. Appl. Phys.* 91 (2002) 2059–2070, <https://doi.org/10.1063/1.1428095>.
- [45] A. Herguth, G. Hahn, Kinetics of the boron-oxygen related defect in theory and experiment, *J. Appl. Phys.* 108 (2010) 114509, <https://doi.org/10.1063/1.3517155>.
- [46] A. Herguth, G. Schubert, M. Kaes, G. Hahn, A new approach to prevent the negative impact of the metastable defect in boron doped CZ silicon solar cells, in: 2006 IEEE 4th World Conf. Photovolt. Energy Conf., 2006, pp. 940–943, <https://doi.org/10.1109/WCPEC.2006.279611>.
- [47] G.M. Wyller, M.S. Wiig, I. Due-Sørensen, R. Sondenå, The influence of minority carrier density on degradation and regeneration kinetics in multicrystalline silicon wafers, *IEEE J. Photovolt.* 11 (2021) 878–889, <https://doi.org/10.1109/JPHOTOV.2021.3078367>.

- [48] A. Graf, A. Herguth, G. Hahn, Determination of BO-LID and LeTID related activation energies in Cz-Si and FZ-Si using constant injection conditions, in: SiliconPV 2019 9th Int. Conf. Cryst. Silicon Photovolt., AIP, 2019, <https://doi.org/10.1063/1.5123890>, 140003-1-140003-5.
- [49] C. Chan, T.H. Fung, M. Abbott, D. Payne, A. Wenham, B. Hallam, R. Chen, S. Wenham, Modulation of carrier-induced defect kinetics in multi-crystalline silicon PERC cells through dark annealing, Sol. RRL 1 (2017) 1600028, <https://doi.org/10.1002/solr.201600028>.
- [50] R. Post, Assessment and Application of Defect Characterization via Lifetime Spectroscopy in High Purity C-Si, Konstanz, 2023. PhD thesis.
- [51] B. Hammann, B. Steinhäuser, A. Fell, R. Post, T. Niewelt, W. Kwapil, A. Wolf, A. Richter, H. Höffler, M.C. Schubert, Quantifying surface recombination—improvements in determination and simulation of the surface recombination parameter J_{0s} , IEEE J. Photovolt. 13 (2023) 535–546, <https://doi.org/10.1109/JPHOTOV.2023.3265859>.
- [52] W. Kwapil, B. Hammann, Hydrogen reactions in c-Si:B during illumination at room temperature, Sol. RRL 7 (2023) 2201107, <https://doi.org/10.1002/solr.202201107>.
- [53] I.L. Repins, D.C. Jordan, M. Woodhouse, M. Theristis, J.S. Stein, H.P. Seigneur, D. J. Colvin, J.F. Karas, A.N. McPherson, C. Deline, Long-term impact of light- and elevated temperature-induced degradation on photovoltaic arrays, MRS Bull. 48 (2023) 589–601, <https://doi.org/10.1557/s43577-022-00438-8>.
- [54] T.H. Fung, M. Kim, D. Chen, C.E. Chan, B.J. Hallam, R. Chen, D.N.R. Payne, A. Ciesla, S.R. Wenham, M.D. Abbott, A four-state kinetic model for the carrier-induced degradation in multicrystalline silicon: introducing the reservoir state, Sol. Energy Mater. Sol. Cells 184 (2018) 48–56, <https://doi.org/10.1016/j.solmat.2018.04.024>.
- [55] A. Herguth, C. Derricks, P. Keller, B. Terheiden, Recovery of LeTID by low intensity illumination: reaction kinetics, completeness and threshold temperature, Energy Proc. 124 (2017) 740–744, <https://doi.org/10.1016/j.egypro.2017.09.090>.